RESEARCH PAPER

CrossMark

Ultimate Strength of Completely Overlapped Joint for Fixed Offshore Wind Turbine Jacket Substructures

Wie Min Gho[1,2] · Ye Yang[3]

Abstract

This paper presents an innovative eccentric jacket substructure for offshore wind turbines to better withstand intense environmental forces and to replace conventional X-braced jackets in seismically active areas. The proposed eccentric jacket comprises of completely overlapped joint at every joint connection. The joint consists of a chord and two braces in a single plane. The two braces are fully overlapped with a short segment of the diagonal brace welded directly onto the chord. The characteristic feature of this joint configuration is that the short segment member can be designed to absorb and dissipate energy under cyclic load excitation. The experimental and numerical study revealed that the completely overlapped joint performed better in terms of strength resistance, stiffness, ductility, and energy absorption capacity than the conventional gap joints commonly found in typical X-braced jacket framings. The eccentric jacket could also be designed to becoming less stiff, with an inelastic yielding and local buckling of short segment member, so as to better resist the cyclic load generated from intense environmental forces and earthquake. From the design economics, the eccentric jacket provided a more straightforward fabrication with reduced number of welded joints and shorter thicker wall cans than the conventional X-braced jacket. It can therefore be concluded based on the results presented in the study that by designing the short segment member in accordance with strength and ductility requirement, the eccentric jacket substructure supporting the wind turbine could be made to remain stable under gravity loads and to sustain a significantly large amount of motion in the event of rare and intense earthquake or environmental forces, without collapsing.

Keywords Offshore wind turbine · Jacket substructure · Eccentric jacket · Completely overlapped joint · Ultimate strength · Cyclic loading · Ductility · Energy absorption

---

Article Highlights
• The completely overlapped joint consists of two braces, which are fully overlapped with a short segment of the diagonal through brace welded onto the chord face directly.
• The short segment member could effectively be designed with inelastic yielding and local buckling to prevent the collapse of wind turbine in the event of intense environmental forces.
• The completely overlapped joint can be performed better with higher strength resistance, stiffness, ductility, and energy absorption capacity than the conventional gap joint.

✉ Wie Min Gho
  cwmgho@gmail.com

1 Maritime Production Research Pte. Ltd, Singapore 915806, Singapore

2 School of Civil and Environmental Engineering, Nanyang Technological University, Singapore 639798, Singapore

3 Global Maritime Consultancy Ltd, London EC2A 2DX, UK

1 Introduction

The design of jacket substructure for offshore fixed wind turbines is primarily based on the recommended practice for designing fixed offshore platforms in the oil and gas industry, such as API RP2A (2000). It is a fixed steel structure directly anchored on the seabed with pile foundation at a water depth of not more than 50 m, and supporting the tower, turbine blades, and facilities. Similar to the structural framing of offshore platforms, the jacket substructure generally is comprised of X-braced vertical framing with welded tubular joint configurations of K-, T/Y-, and X-joints, as illustrated in Fig. 1a. Depending on the magnitude of environmental forces, it might consist of horizontal braces to enhance its flexural rigidity.

The jacket substructure is basically subjected to a large wind load from the turbine in both the operating and off-service conditions, additionally to wave and current. These loadings will eventually be transferred through the diagonal braces from the top framing of the jacket substructure to its
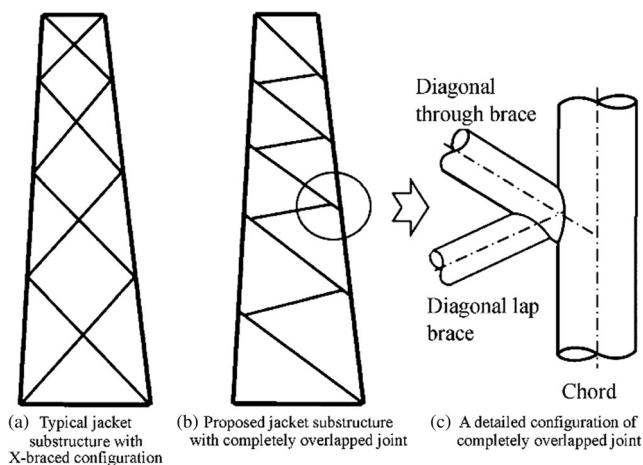
Fig. 1 Jacket substructures of offshore wind turbine

foundation. In the process of load transfer, the welded tubular joints play a significant role to transmit effectively the loads from members to members. Thus, the ultimate capacity and fatigue resistance are generally the basic criteria for sizing the joints for all possible load cases so that they can be performed satisfactorily under service conditions and to achieve a reasonable balance between economy and risk of failure.

However with increasing demand on the use of wind energy offshore to generate electricity in recent years, particularly in deeper waters where wind power is substantial and steadier, researchers and engineers are seeking solutions for better structure system to reduce capital investment associated with fabrication and installation of wind turbines.

This paper therefore proposes an eccentric jacket substructure for design economics of offshore fixed wind turbines to better withstand intense environmental forces and to replace conventional X-braced jackets in seismically active areas. The proposed eccentric jacket is comprised of completely overlapped tubular circular hollow section joint (hereafter as completely overlapped joint) at every joint connection, as shown in Fig. 1b. The detailed configuration of the completely overlapped joint is highlighted in Fig. 1c.

In comparison to the typical X-braced jacket (Fig. 1a), the eccentric jacket possesses several advantages in terms of load transfer mechanism and reduced number of welded joints and shorter thicker wall cans for fabrication. Unlike the gap or partially overlapped K-joint of X-braced jackets, where the joint failure generally occurs on the chord wall, the failure of the completely overlapped joint is merely located at the short segment of the diagonal through brace that welded onto the chord. This short segment member can be designed to dissipate and absorb energy generated by load excitation. The inelastic yielding and local buckling of the short segment member also enable the jacket substructure to remain stable under gravity loads and to sustain intense environment forces or earthquake without collapsing after yielding.

As most of the research work done of completely overlapped joints is carried out under static loads within the elastic limit of materials, this paper will present in detail the experimental and numerical study on the inelastic performance of the joint under cyclic loading. The need for reliable numerical technique to supplement experimental study for analysis of this joint configuration is also presented. Finally, a comparison of failure behaviour with the gap joint commonly used in conventional X-braced jacket, together with the two idealised cases of joints without gap and 100% overlapped, is conducted to demonstrate the merit of incorporating the completely overlapped joint in the eccentric jacket substructure framing.

In this paper, the fatigue assessment of the eccentric jacket is not covered. It will be carried out in future work with a full coupled analysis reference to the evaluation of fatigue damage model prediction by Yeter et al. (2016).

2 Completely Overlapped Joint

The geometrical parameters of the completely overlapped joint are defined in Fig. 2. It consists of two (2) braces fully overlapped with a short segment of diagonal brace of gap size (g) welded directly onto the chord wall.

2.1 Design Economics

From the literature review, the concept of eccentric jacket with completely overlapped joint for offshore platforms was first introduced by engineers from McDermott SEA Pte Ltd. (Cheung et al. 1998). They proposed eccentric jacket to reduce
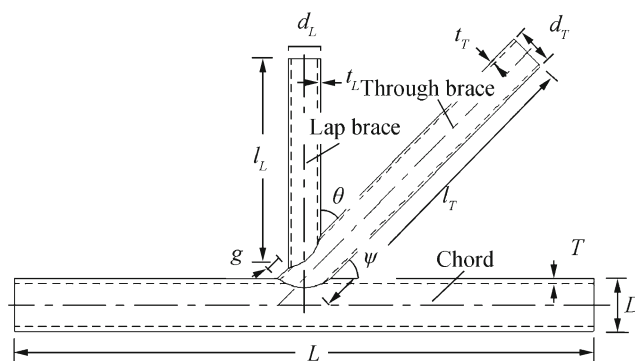
Chord length (L), Chord diameter (D), Chord thickness (T),
Through brace length (l_T), Through brace diameter (d_T),
Through brace thickness (t_T), Lab brace length (l_L),
Lap brace diameter (d_L), Lap brace thickness (t_L),
Brace angle between lap and through braces (θ),
Brace angle between through braces and chord (ψ)
Non-dimensional parameters :
$\alpha_C = 2L/D$, $\gamma_C = D/2T$, $\alpha_T = 2l_T/d_T$, $\gamma_T = d_T/2t_T$,
$\beta_{CT} = d_T/D$, $\tau_{CT} = t_T/T$, $\beta_{TL} = d_L/d_T$, $\tau_{TL} = t_L/t_T$

Fig. 2 Geometrical parameters of completely overlapped joint

project cost and to improve work schedule by designing a structure which was suitable for fabrication and installation. Based on the cost analysis and analytical investigation, they commented that the eccentric jacket could function well as conventional X-braced jacket in non-earthquake area, where the design criteria were governed by 100-year storm wave. It was found to be lighter in weight and more economical for fabrication, with 25% reduction of main steel fabrication man-hours. They further commented that if the X-braced jacket was to replace with the eccentric jacket in seismically risk areas, and the design was based on elastic limit of materials for both strength and ductility level earthquake, then the saving of fabrication and material costs could be substantial.

Despite the design economics of the current proposed eccentric jacket for offshore fixed wind turbine has not been examined, the study by Cheung et al. (1998) however highlighted that the saving of fabrication man-hours and material costs could be expected, in view of the reduced number of welded tubular joints and shorter thicker wall joint cans as well as the joint failure behaviour, in comparison to the conventional X-braced jacket.

2.2 Research and Development

Most of the research work of completely overlapped joints has been focused on the ultimate strength and stress concentration for joint design. The experiment of large-scale completely overlapped K(N)-joint specimen (457 mm chord diameter) under lap brace axial compression conducted by Fung et al. (2001) concluded that the joint ultimate capacity was comparable to that of the gap K(N)-joint. The joint failure was the through brace wall plastification. The chord wall deformation at joint failure was found to be minimal. The experimental research on the stress and strain concentration of large-scale completely overlapped joint by Gho et al. (2003) commented that the maximum stress and strain concentrations occurred at the through brace saddle, and not the chord wall, at the joint intersection of the through brace and the lap brace.

A detailed parametric study conducted by Gho and Yang (2008) and Gao and Gho (2008) based on the finite element (FE) joint models after verified with two small-scale completely overlapped joint specimens (273 mm chord diameter) derived a set of parametric equations to predict the static strength and the stress concentration factor (SCF) of the joint. The conclusions of their study were that the short segment of the diagonal brace of the completely overlapped joint controlling the joint failure behaviour. The ultimate strength and the SCF of the joint at small and large gap sizes were found comparable to that of gap K-joint and that of simple Y-joint, respectively.

From the parametric study based on 1296 joint models carried out by Gho et al. (2006), the failure modes of the completely overlapped joint under lap brace axial compression could be classified as the through brace wall plastification, lap brace yielding, lap brace local buckling, and lap brace member failure, as illustrated in Fig. 3. It is important to realise that the joint failure was not occurred on the chord wall.

Apart from the ultimate strength and the stress concentration, the local joint flexibility of the completely overlapped joint under lap brace loading conducted by Gho (2009) commented that the through brace axial and bending loads resulted in axial and rotational deformation on the chord wall. These loadings were transferred to the chord wall via the shell bending, beam action, or combined shell and beam behaviour dependent upon the geometrical properties of the short segment of the diagonal through brace at the joint. A set of parametric equations was subsequently derived by Gao et al. (2013) to predict the local joint flexibility for assessment of eccentric jacket under dynamic loading.

For the research on cyclic behaviour, Soh et al. (2001) performed experimental study of a large-scale completely overlapped joint specimen under cyclic quasi-static loading. Their study revealed that the hysteresis performance of the joint could be improved by increasing the lap brace diameter. However, the gap size of short segment and the through brace wall thickness showed limited effect. Based on the same experimental result for verification, the parametric study carried out by Gho and Yang (2005) commented otherwise that the short segment of diagonal brace was an important element controlling the failure mechanism of the joint under cyclic loading. Nevertheless, the research work for the joint under cyclic loading was still quite limited. Extensive study of the subject is essentially required to better understand the cyclic performance of the joint.

(a) Through brace wall plastification

(b) Lap brace yielding

(c) Lap brace local buckling
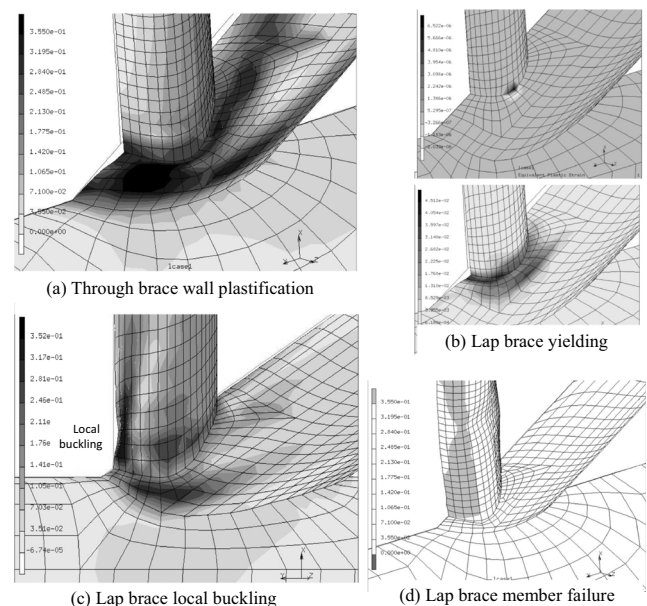
(d) Lap brace member failure

Fig. 3 Failure mode of completely overlapped joint

The seismic performance of a structure would depend on its inelastic cyclic response. The dissipative zone of a structure under hysteretic behaviour could be designed based on material yielding and member buckling for dissipating the energy. The dissipative zone was therefore designed to have adequate ductility and strength to resist the load (British Standard Institution, BSI 1998). The key parameter to measure the seismic efficiency of steel components in a frame was the ability to dissipate energy by undergoing a large plastic deformation without failure.

For the eccentric jacket substructure, the dissipative zones were found located near the end of diagonal through brace of the completely overlapped joint. Thus, the ductility and the energy dissipation capacity of the joint under cyclic loading at large plastic deformation were investigated. In the current study, the test of the joint specimen was carried out to verify the reliability of the FE model for detailed analysis. The assessment approach to measure the performance and the sensitivity study of the FE models for the joint under cyclic loading was described in detail and presented in the following sections.

3 Assessment of Cyclic Behaviour

A tubular joint under cyclic loading could be considered stable if it exhibited the same behaviour as that under monotonic loading based on the area of hysteresis loops with increasing load cycles. On the contrary, it could be considered unstable if its stiffness decreased with load cycles characterised by continuously decreasing slopes in the hysteresis curves. Hence, the joint under cyclic loading was ideal at specific strength level with no deterioration of stiffness after a number of load cycles.

The evaluation of the joint performance under cyclic loading was based on several behavioural parameters, namely the ductility, strength resistance, stiffness, and energy dissipation. These parameters can be obtained through a comparison between the generic and the corresponding ideal elastic-perfectly plastic cycles with the same displacement amplitude, as shown in Fig. 4.

3.1 Ductility

In ultimate capacity design, steel structures were generally classified based on ductility index (μ) into three categories, namely the fully ductile, limited ductility, and fully elastic as specified in CSA (1989) and NZS (1992). In the current study, an indicator was introduced based on the ductility ratio to determine the ductility performance of the joint under cyclic loading, as follows:

$$\mu = \delta_{\max}/\delta_y \tag{1}$$

where $\delta_{\max}$ and δ_y denoted the maximum and yield deformation of joints prior to excessive loss of resistance and for ideal elastic-perfectly plastic behaviour, respectively. In NZS (1992), the collapse of structures under cyclic loading was assessed based on 20% reduction strength in load-deformation curve. For the cyclic behaviour, the ductility ratio at ith half-cycle could be defined as

$$\mu_i^+ = \delta_i^+/\delta_y^+ \cdot (\text{Tension phase}) \tag{2}$$

$$\mu_i^- = \delta_i^-/\delta_y^- \cdot (\text{Tension phase}) \tag{3}$$

where δ_i^+ and δ_i^- were the maximum displacements at ith tension and compression, δ_y^+ and δ_y^- were the yield displacements in tension and compression half-cycle, respectively, for ideal elastic-perfectly plastic behaviour. It could therefore be seen from the above formulation that the joint capacity beyond the elastic limit of material at large deformation increased with ductility ratio.

It was recommended to adopt the first development of localised inelastic strain, significant yielding or buckling in critical members or overall loss of structure stiffness if δ_y could not be identified. From the load-deformation relationship obtained in the current test result, the overall loss of joint stiffness was taken as the yield displacement.
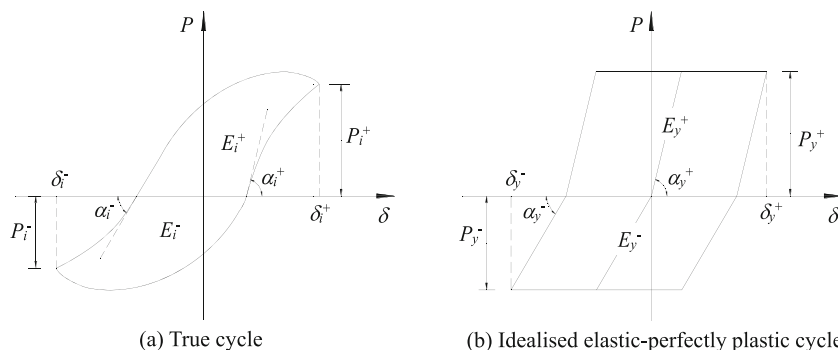

(a) True cycle   (b) Idealised elastic-perfectly plastic cycle

Fig. 4 Basic parameters of load cycle

ECCS ([1986]) specified several methods to determine the yield displacement of structures. The appropriate method to be adopted for assessing the joint capacity under cyclic loading in accordance with the load-deformation curve under monotonic loading was summarised as follows:

(i) Yield force corresponding to first yield of test specimen (Fig. 5a).

(ii) Yield force corresponding to ultimate capacity of test specimen (Fig. 5b).

(iii) Yield force corresponding to yield deformation in inelastic region. The yield deformation is equivalent to two times the elastic deformation as illustrated in Fig. 5c.

(iv) Yield force corresponding to intersection of two tangent lines plotted in elastic and inelastic regions, as shown in Fig. 5d. The tangent of the curve in the inelastic range was based on a slope equivalent to 1/10 of that in the elastic region.
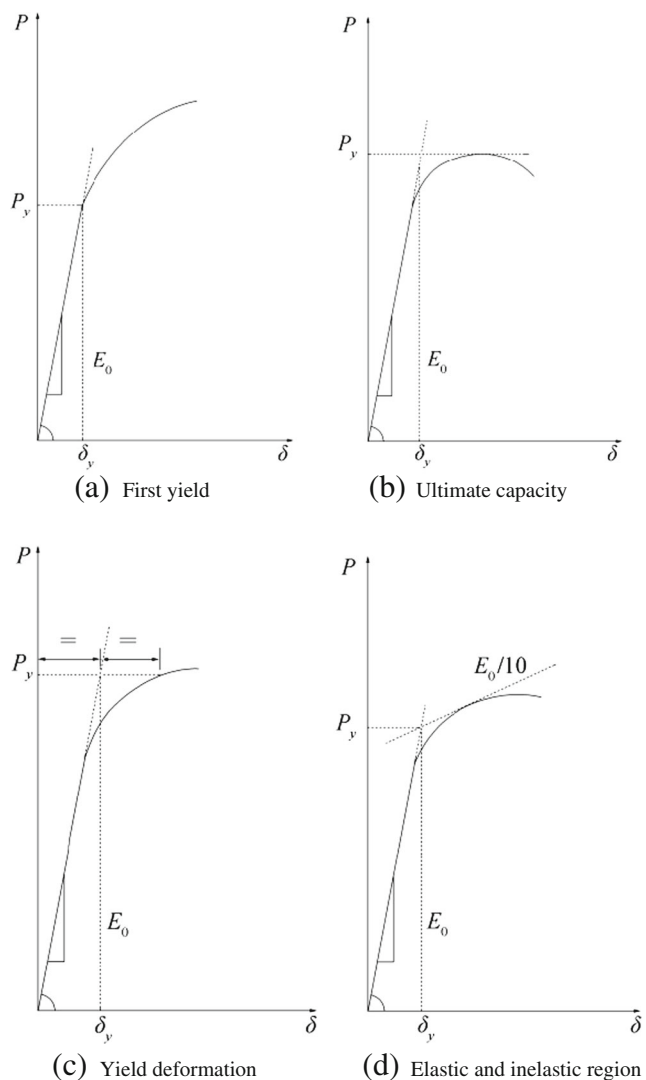
Fig. 5 Determination of yield force and displacements

(a) First yield

(b) Ultimate capacity

(c) Yield deformation

(d) Elastic and inelastic region

(v) In other cases, the yield displacement was obtained from numerical computation.

The abovementioned methods for assessing the joint capacity under cyclic loading possessed advantages and disadvantages. For method (i), the post yield region of the curve was ignored. For method (ii), the buckling mode was captured, and this was corresponded to the excessive deformation of flexural behaviour of members or joints. On the contrary, the deformation of members and joints was well defined in method (iii). ECCS ([1986]) however recommended the use of method (iv) for all cases. Method (v) was only applicable for cases where the design resistances were precisely determined based on test data. In the current study, method (iv) recommended by ECCS ([1986]) was adopted.

In some cases, the required level of displacement of the test specimen could not be achieved owing to the limitation of the test facility in the laboratory. In order to complete the full cycle of test procedure, the loading was applied with identical displacement amplitude. Under this circumstance, the ductility ratio (μ) might not be able to defined using the maximum displacement. A more realistic approach to assess the cyclic performance was therefore to measure the accumulative ductility of the joint under cyclic loading, defined as the summation of ductility ratio of each cycle as follows:

$$\mu_a = \sum_{i=1}^{N_c} \left(\mu_i^+ + |\mu_i^-| \right) \tag{4}$$

where N_c was the total number of load cycles.

3.2 Strength Resistance

For a large inelastic displacement cycle in hysteresis curves, the strength decreased after the material yielded due to the damage of structural elements at the joint such as local buckling, material yielding, plastification, cracking, or a combination of these effects. Under this circumstance, the reduction of strength resistance of the structural element could be evaluated using the strength resistance ratio as shown below:

$$\omega = P_i / P_y \tag{5}$$

where P_i and P_y were the force magnitude at point of unloading at ith cycle and the yield force for idealised elastic-perfectly plastic behaviour, respectively. Similar to the previous definition of μ_i^+ and μ_i^-, the respective strength resistance ratios in tension and compression half-cycle could be defined as follows:

$$\omega_i^+ = P_i^+ / P_y^+ \cdot \text{(Tension phase)} \tag{6}$$

$$\omega_i^- = P_i^- / P_y^- \quad \text{(Compression phase)} \tag{7}$$

where P_i^+ and P_i^- were the force magnitudes at point of unloading and P_y^+ and P_y^- were the yield forces in tension and compression half-cycle, respectively, for idealised elastic-perfectly plastic behaviour.

3.3 Joint Stiffness

The joint stiffness deteriorated with increasing number of load cycles, mainly caused by the global and local buckling phenomena such as the Bauschinger effect exhibited in steel material subjected to inelastic load reversals or residual curvature during load cycles. Thus, the stiffness ratio for assessing the joint behaviour could be expressed as follows:

$$\zeta_i^+ = \tan\alpha_i^+ / \tan\alpha_y^+ \cdot (\text{Tension phase}) \tag{8}$$

$$\zeta_i^- = \tan\alpha_i^- / \tan\alpha_y^- \cdot (\text{Compression phase}) \tag{9}$$

where $\tan\alpha_i^+$ and $\tan\alpha_i^-$ were the slope of tangent lines in hysteresis loops with forces change at ith load cycle, from negative to positive and positive to negative, respectively. These parameters for idealised elastic-perfectly plastic behaviour were the increased forces on the respective positive and negative side of the curve.

3.4 Energy Dissipation

In an intense earthquake or environmental forces, the elastic limit of joint capacity could be exceeded and the structure became a mechanism of energy dissipation. The area enclosed by hysteresis loop (E_i) at ith cycle was the amount of energy dissipated during the load history. The energy dissipation efficiency of the joint could therefore be measured based on the energy dissipation ratio as follows:

$$\eta_i^+ = E_i^+ / E_y^+ \cdot (\text{Tension phase}) \tag{10}$$

$$\eta_i^- = E_i^- / E_y^- \cdot (\text{Compression phase}) \tag{11}$$

where E_i^+ and E_i^- were the dissipated energy in tension and compression phase of ith cycle and E_y^+ and E_y^- were the dissipated energy in tension and compression phase for idealised elastic-perfectly plastic behaviour, respectively. They could be computed using the following formulae:

$$E_y^+ = P_y^+ \left(\delta_i^+ - \delta_y^+ + \delta_i^- - \delta_y^- \right) \tag{12}$$

$$E_y^- = P_y^- \left(\delta_i^- - \delta_y^- + \delta_i^+ - \delta_y^+ \right) \tag{13}$$

Alternatively, a more useful and realistic parameter to determine the accumulative energy dissipation ratio highlighted by Soh et al. (2001) could be adopted.

$$\eta_a = \sum_{i=1}^{N_c} \left(E_i^+ + E_i^- \right) / E_y \tag{14}$$

where E_y was the energy absorption at first yield displacement (δ_y) of the joint defined as $E_y = P_y \delta_y / 2$.

From the above, all the parameters except those in accumulative ratio were defined based on the idealised elastic-perfectly plastic material behaviour obtained in the experiment. Generally, the joint behaviour followed closely the actual material with the condition that the formulae for assessing the joint capacity under cyclic loading with value approaching unity. In summary, the limiting values derived from these parameters could be utilised in the ultimate limit state for design of tubular joints under cyclic loading. A small value of these ratios computed from the formulation indicated a substantial loss of strength, stiffness, and/or energy dissipation of a joint.

4 Experimental Investigation

In the experiment, two completely overlapped tubular K(N)-joint specimens were tested to failure under monotonic axial compression and quasi-static cyclic loading. The geometrical properties of these two test specimens are identical with the setup in the rig as shown in Fig. 6. The joint specimen is comprised of a chord, a 30° diagonal through brace and a vertical lap brace. The geometrical properties of the joint specimens are listed in Table 1. Both ends of the chord and the through brace are welded directly onto the flat plates and then bolted onto the rig. A gap size (g) of clear distance 143 mm was measured at the short segment of the diagonal through brace on the chord. The vertical static and cyclic loads were applied at the lap brace end using a double-acting hydraulic controlled cylinder. The test of the two joint specimens was conducted in the laboratory at Nanyang Technological University of Singapore. A detailed description of the test setup with the measurement of displacement and axial and principal strains at the joint intersections for analysis was compiled by Yang (2006).

The first specimen was tested to failure under axial monotonic compression. The test results were used to verify the joint FE model for predicting the strength and stiffness of the completely overlapped joint and for reference with that of the joint under cyclic loading. As illustrated in Fig. 7, δ_y and δ_u were the displacements corresponding to the first yield and peak load obtained from the first joint specimen.

The second joint specimen was tested to failure under axial quasi-static cyclic loading. In the test, the joint specimen was initiated by five elastic displacement amplitudes, $\pm 0.125\delta_y$, $\pm 0.25\delta_y$, $\pm 0.375\delta_y$, $\pm 0.5\delta_y$, and $\pm 0.75\delta_y$. Each of these values represent a single load cycle as shown in Fig. 8. This was
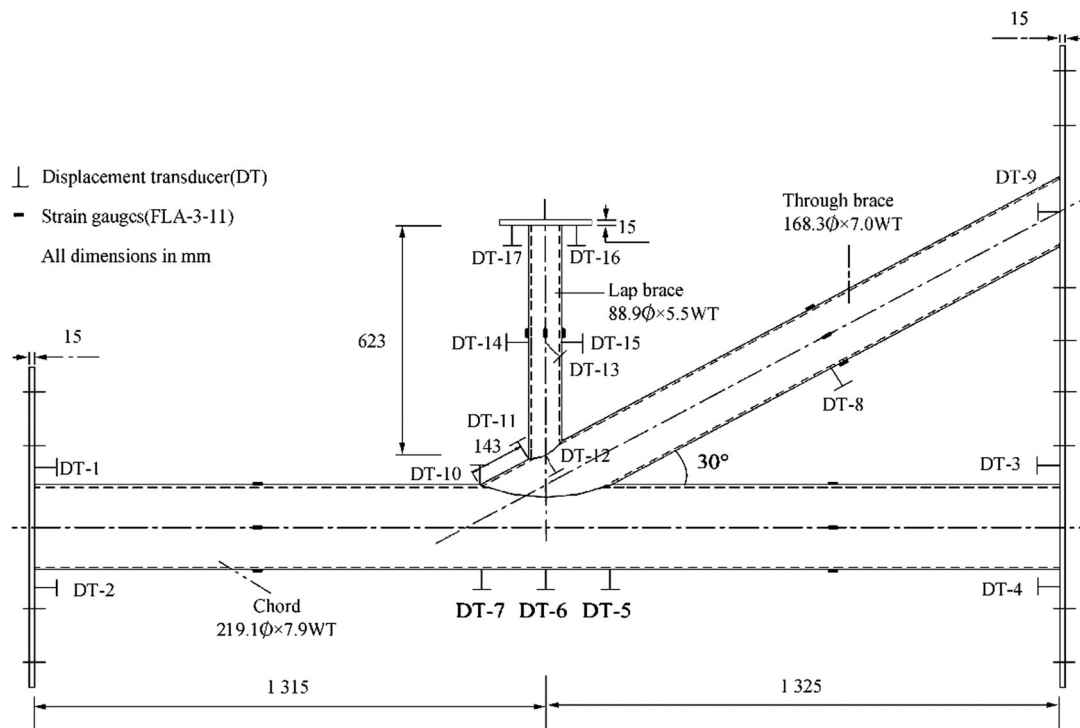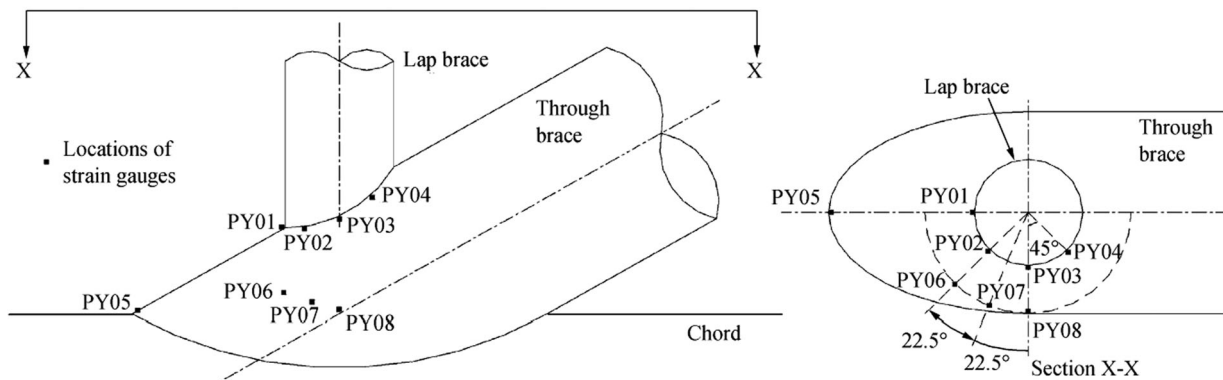
(a) Position of displacement transducer on joint specimen
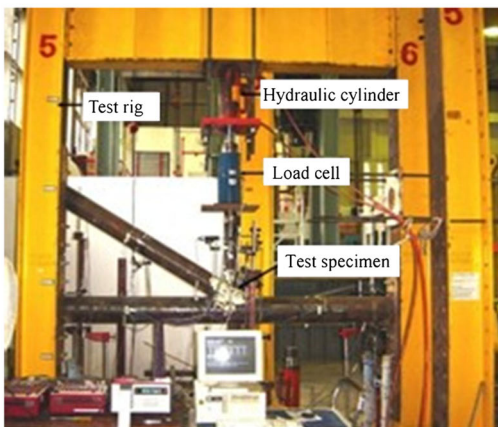
(b) Setup of joint specimen
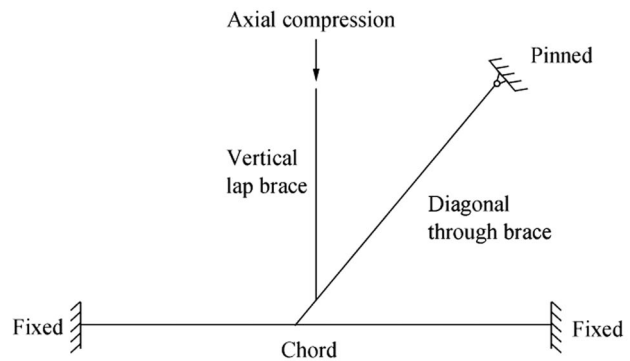
(c) Applied load on joint specimen

(d) Locations of rosette strain gauges (YEFRA-2) on joint specimen tested under cyclic loading

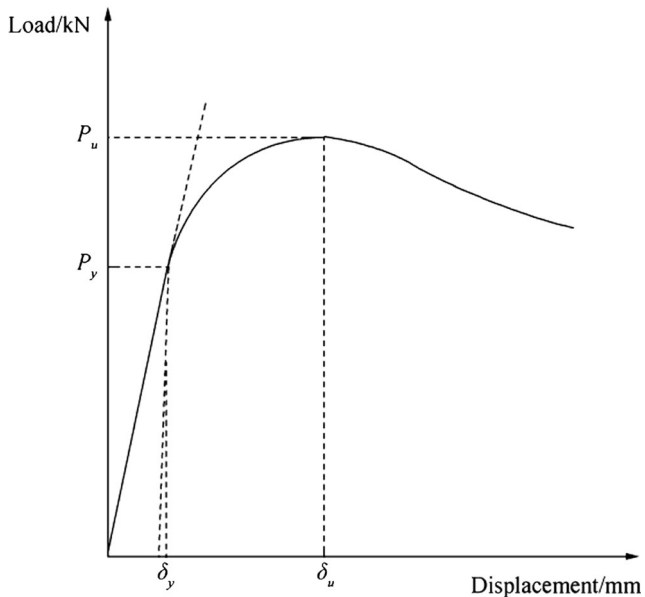**Fig. 6** Experimental setup of joint specimen on the rig

Table 1 Geometric parameters of test specimen, unit: mm

Chord length, L	2640.0
Chord diameter, D	219.1
Chord thickness, T	7.9
Through brace length, l_T	1870.0
Through brace diameter, d_T	168.3
Through brace thickness, t_T	7.1
Lab brace length, l_L	623.0
Lap brace diameter, d_L	88.9
Lap brace thickness, t_L	5.5

Non-dimensional parameters of the joint configuration: $\alpha_C = 2L/D = 24.10$, $\gamma_C = D/2T = 13.87$, $\beta_{CT} = d_T/D = 0.77$, $\tau_{CT} = t_T/T = 0.90$, $\alpha_T = 2l_T/d_T = 22.22$, $\gamma_T = d_T/2t_T = 11.85$, $\beta_{TL} = d_L/d_T = 0.53$, $\tau_{TL} = t_L/t_T = 0.77$, $\xi = g/d_T = 0.85$

followed by displacement amplitude $\pm\delta_y$ in one load cycle. The tension displacement was constant at amplitude $\pm\delta_y$ in view of the rig capacity. The compression displacement amplitudes were increased to $-1.25\delta_y$, $-1.5\delta_y$, $-2.0\delta_y$, and $-2.5\delta_y$. The load control mode in tension range increased from 250 to 270 kN. The compression displacement with three load cycles was remained constant at $-3\delta_y$. Finally, the test terminated at compression displacement equivalent to 1.5 times the peak load (δ_u) of the specimen tested under monotonic axial compression. The quasi-static cyclic loading protocol used in the current experiment was designed in accordance with the guideline specified by ECCS (1986).
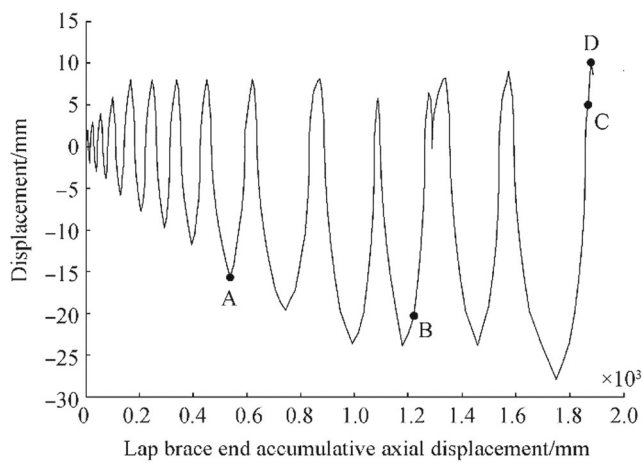
The load response and the axial displacement of the lap brace for the joint specimen tested under cyclic loading are plotted in Fig. 9. In the figure, the x-axis is the accumulative absolute displacement measured at the lap brace end. In the compressive phase, a significant local buckling of through
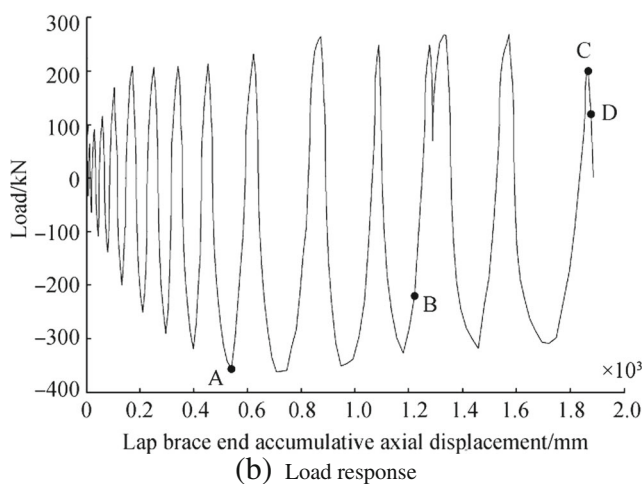

Fig. 8 Displacement-time (cyclic load)

(a) Displacement history

(b) Load response

Fig. 9 Load response and axial displacement (cyclic load)

Fig. 7 Load-displacement (monotonic load)

brace wall occurred at load cycle 9th (point A). The load and the displacement at this point were 357 kN and 15.65 mm, respectively. A permanent deformation of 3.06 and 2.39 mm was recorded after the joint was unloaded.

The tension responses of the joint specimen at load cycles 5th to 9th were almost identical. However, the force responses significantly increased after the next two load cycles. This behaviour revealed that the impact of the joint tensile strength in the compression range was minimum prior to the displacement $-3\delta_y$, and it was affected by the local buckling of compression member.

At load cycle 12th, the compression force and the corresponding axial displacement were 220.5 kN and 20.3 mm (point B), respectively. On the through brace saddles, the cracks at points C1 and C2 were about 7 mm and 5 mm (Fig. 10). These two cracks occurred symmetrically about the vertical plane of the joint specimen. With an increasing load cycles, the cracks propagated along the perimeter toward the heel and the toe of the joint. A sound "bang" was subsequently heard at load cycle 14th, as the lap brace separated from the through brace. At this time, the load was in the tension zone (point C). It drastically reduced from 201 to 120 kN with increasing axial displacement from 5.1 to 10.1 mm (point D). At this load level, the joint specimen was considered completely collapsed. The joint ultimate capacity in the tension and compression phases was recorded as 270 kN and 362 kN, respectively.

The joint specimen was considered failed in tension half-cycle at accumulative displacement of 1868.6 mm (point C, Fig. 9). At this point of loading, the crack penetrated through the through brace wall resulting in a sudden drop of strength by 40.3%. The cracks initiate at the through brace saddles at points C1 and C2, as shown in Fig. 10. An inelastic local buckling failure of the through brace wall at the joint was clearly observed. A detailed investigation after the test revealed that no other parts of the test specimen, except the joint intersection of the through brace and the lap brace, were found damage.
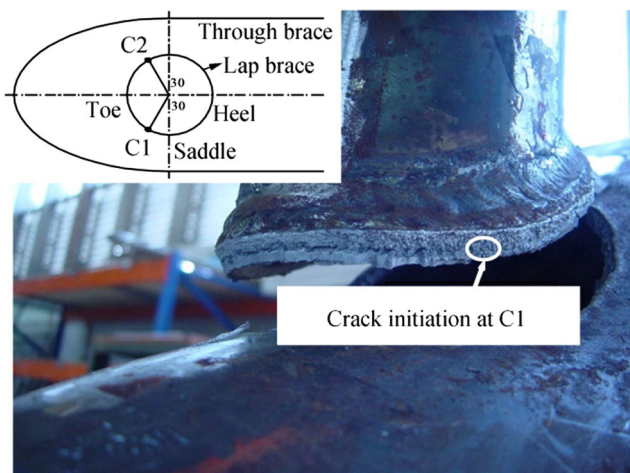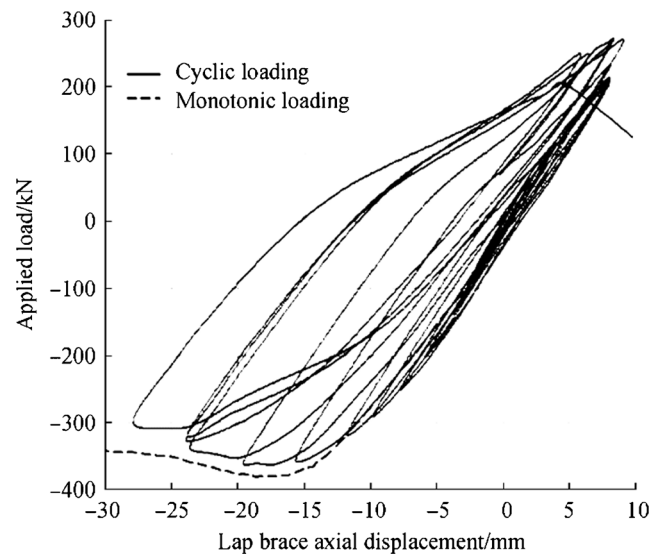

Fig. 11 Load-displacement curves of joint specimen

The load-displacement hysteresis curve of the joint specimen tested under cyclic loading is plotted in Fig. 11. In the current study, the load-displacement curve of the joint specimen tested under monotonic axial compression served as an upper bound of load level for the compressive range of the hysteresis curve.

The comparison of the load-displacement curves as shown in Fig. 11 indicated that the force response of the joint specimen under monotonic axial compression is higher than that under cyclic loading. The difference of the force response for the two joint specimens was due to the effect of material deterioration at the joint intersection of the through brace and the lap brace under the load reversal. It could be commented that the joint specimen under monotonic axial compression could form a reasonable envelope for the joint under cyclic loading at the first load cycle of $3\delta_y$. Thereafter, the joint strength
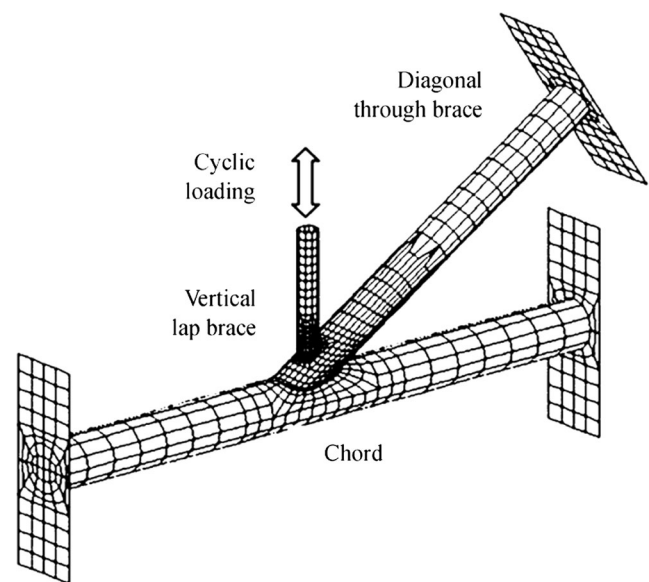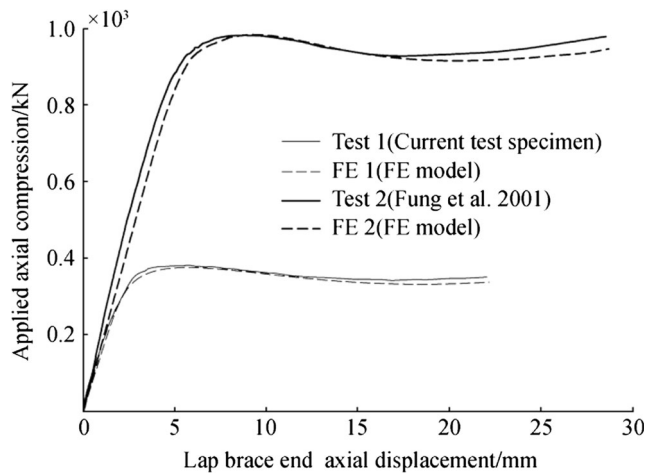

Fig. 10 Crack initiated at through brace saddle

Fig. 12 FE model of joint specimen

Fig. 13 Load-displacement (monotonic compression)

(a) Failure behavior of joint specimen   (b) FE model of joint specimen

Fig. 15 Through brace wall plastification

degraded with increasing load cycles. The failure load of the joint specimen under cyclic loading was found lower than that of the joint under monotonic axial compression.

5 Finite Element Modelling

5.1 Modelling Technique

A commercial FE package MARC with pre- and post-processing program MENTAT was adopted for the investigation of completely overlapped joint behaviour under lap brace axial cyclic loading (MARC 2000). For verification, the geometrical, material, and dimensional properties of the joint model were identical to those of the joint specimen presented in Section 4.

In the modelling, the mid-plane of member wall thickness is modelled using thick shell element, as illustrated in Fig. 12. The cyclic load applied at the lap brace end was displacement control mode. A relatively high density of meshes at the joint intersections of members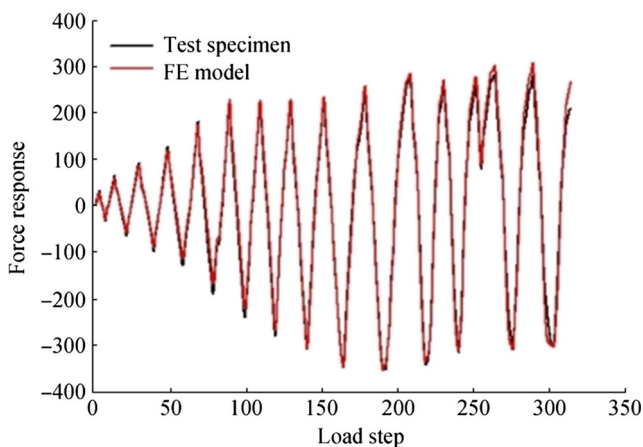 was considered to account for the effect of high stress gradients. The size of finite element increased with distance outside the joint region.
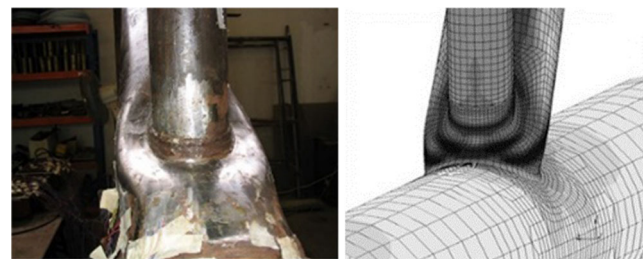
The material and the geometric non-linearities of the joint model were considered in the analysis. Young's modulus, the yield stress, and the ultimate tensile stress of the members of the joint were obtained from the tensile coupon tests (Yang 2006). Poisson's ratio was taken as 0.28. The true stress and the logarithm strain were adopted to account for large strain effect of material properties. The von Mises yield criterion and the multi-linear work hardening rule of plasticity were applied. A large displacement with updated Lagrange procedure and the finite strain plasticity were activated for a complete large strain plasticity formulation. A full Newton-Raphson method was the approach to reassemble the stiffness matrix of load iteration in displacement control mode. The convergence criteria for residual force and moment relative to reaction force and moment were set at 5%.

As shown in Figs. 13, 14, and 15, the joint model simulates very well the load-displacement and the force response-load step relationships of the two joint specimens, under monotonic axial compression and cyclic loading, respectively. A comparison with the previous test results by Fung et al. (2001) based on a large-scale joint specimen (457 mm chord diameter) also showed a good agreement. The difference of the joint ultimate capacity between the test specimens and the FE model under the monotonic axial compression and cyclic load conditions was found less than 3.5% and 5%, respectively.
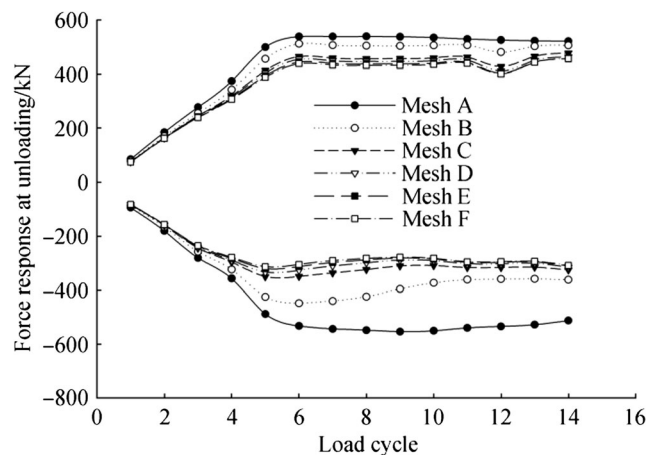

Fig. 14 Force response-time step (cyclic loading)

Fig. 16 Convergence study of mesh density

Table 2 Element sizes at joint intersections, unit: mm

Mesh density	Chord	Diagonal brace	Horizontal brace
A	110.60	63.90	24.75
B	55.30	24.85	11.00
C	31.60	17.75	6.60
D	23.70	14.20	5.50
E	15.80	7.10	2.75
F	11.85	3.55	2.75

5.2 Convergence Study

A convergence study was conducted based on six different mesh densities to derive a sufficiently fine mesh of the joint model for accurate solutions. The force response at the unloading point of each load cycle of different mesh layouts is presented in Fig. 16. The results converged as the FE mesh became finer. The FE mesh D was found more suitable for simulating the joint model under cyclic loading with a balance of element sizes and computational effort (Tables 2 and 3).
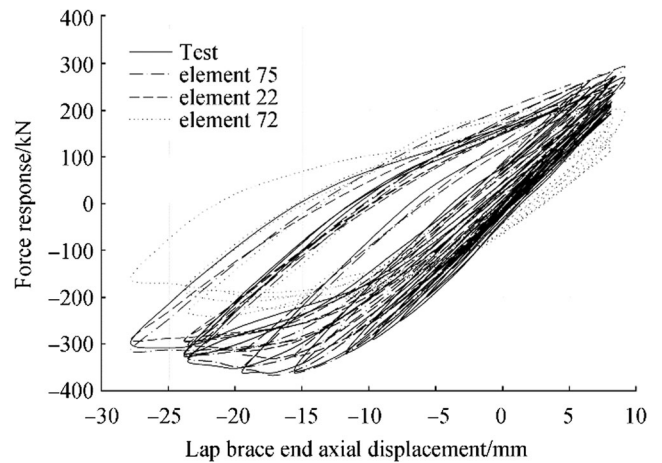
5.3 Finite Element Type

From the comparison of hysteresis curves as shown in Fig. 17, both four- and eight-node thick shell element (types 75 and 22, respectively) are suitable for modelling the joint with sufficient accuracy. Four-node thin shell element (type 72) was unsuitable as the effect of transverse shear was not included. Despite the joint model with eight-node thick shell element type 22 yielded lower force response, the average difference of cyclic response of the models with the two (2)-thick shell elements was less than 5%. In view of the computational effort, the four-node thick shell element type 75 was adopted in the current study.

5.4 Effect of Weld Elements

The joint model without the weld elements yields a lower response (Fig. 18). The difference of the force response of the joint model with and without the weld elements in the respective compression and tension phases of load cycle

Fig. 17 Effect of element types

was 5.5% and 3.5%, respectively. The weld profile was determined based on the dihedral angle along the joint perimeter specified by AWS (2000). However, the weld profile was somewhat arbitrary unless the actual weld size at the joint was measured. In view that the difference of the force response for the joint with and without the weld element was small, and to generate a more conservative result for assessment, the weld element was not considered in the joint model.

5.5 Effect of Material Properties

The isotropic and the kinematic hardening rule was considered for modelling the material post yield properties of the joint model. As shown in Fig. 19, the isotropic hardening model overestimates the maximum joint capacity. Besides, the deterioration of joint strength increasing with load cycle could not be identified. The reason was that the isotropic hardening model excluded the Bauschinger effect due to plastic deformation. Thus, the elastic range of the material expanded with equivalent plastic strains. The kinematic hardening model however predicted accurately the cyclic behaviour of the joint. In the current study, a multi-linear kinematic hardening material model was adopted for modelling the post yield behaviour of the completely overlapped joint under cyclic loading.
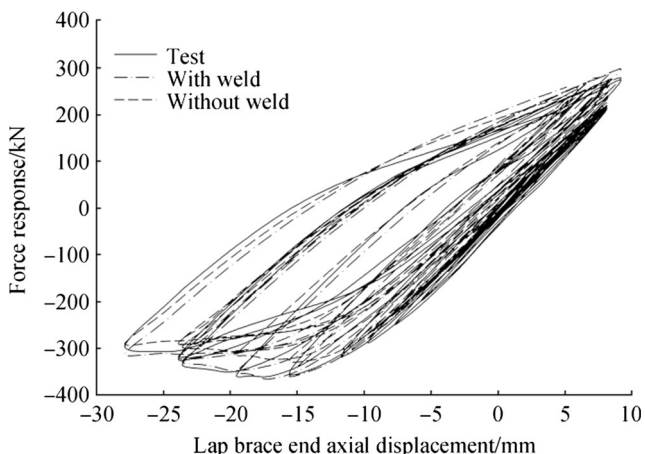
Table 3 Element (ultimate load and CPU time)

Mesh density	No. of elements	No. of nodes	Ultimate load/kN	CPU time/s
A	161	195	565.3	46
B	417	479	415.8	135
C	959	1045	368.1	306
D	1900	2019	351.0	682
E	4115	4263	349.8	1736
F	7948	8113	348.9	3110

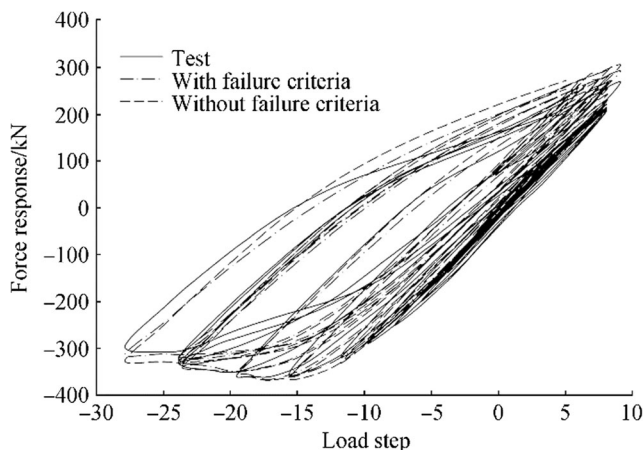**Fig. 18** Effect of weld elements

5.6 Effect of Failure Criterion

A maximum tensile stress of 486 MPa, which was the ultimate tensile stress of the through brace obtained from the tensile coupon test (Yang 2006), was taken as the failure criterion to simulate the crack initiation of the joint model. This failure criterion was only applied to finite elements at the weld toe vicinity at the joint intersection of the through brace and the lap brace. At failure, the material property of these elements was taken as 10% of Young's modulus. The hysteresis curves of the test specimen and the FE model with failure criterion presented in Fig. 20 show that the joint tensile capacity is 3.3% lower. The joint compressive resistance was not affected as the failure was not associated with cracking.

6 Comparison with Gap Joint

In order to assess the structural performance, the hysteresis behaviour of completely overlapped joint was compared with that of similar kind of gap joint configuration commonly
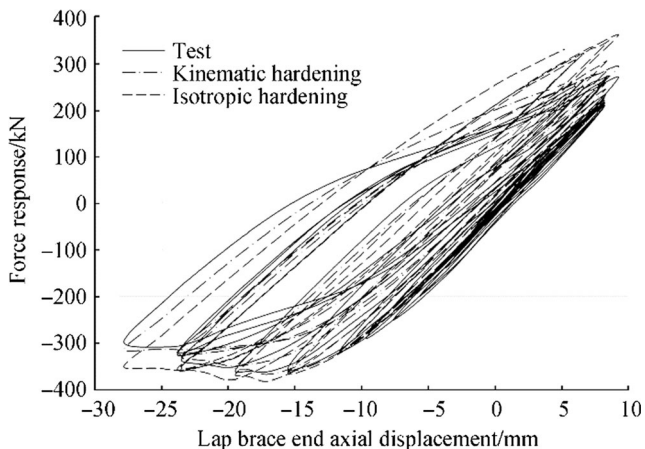

Fig. 19 Effect of material properties

Fig. 20 Effect of failure criterion

found in X-braced jacket substructures. As illustrated in Fig. 21 on the K(N)-joint configurations, the gap size between the two braces on the chord face of the gap joint was identical to that of the short segment of the diagonal through brace on the chord of the completely overlapped joint. Additional two cases of idealised joint configurations without gap and 100% overlapped were included to present the upper bound of joint
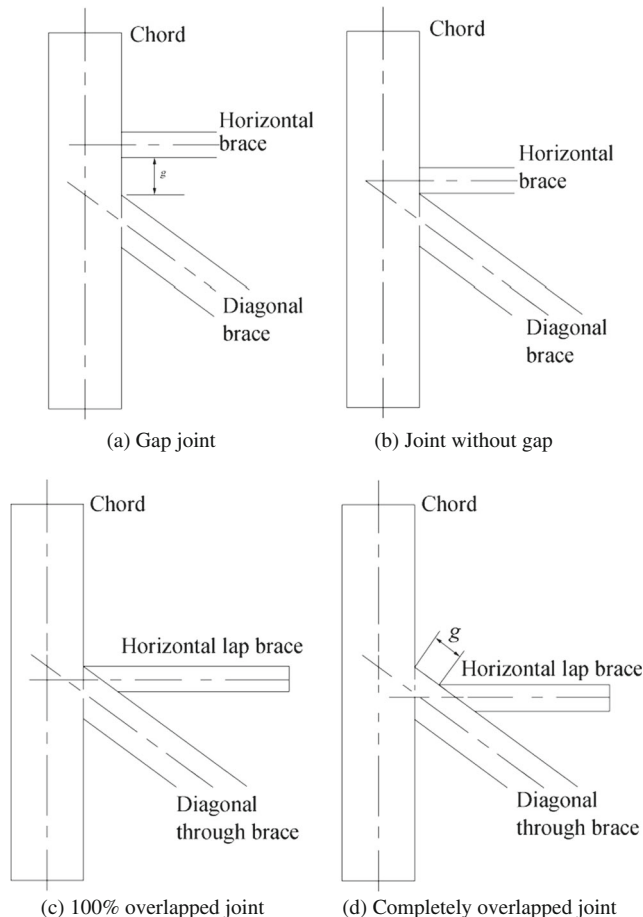

Fig. 21 Four K(N)-joint configurations

capacity for reference. These two joint configurations however not representing the actual condition as the overlapping of weld at joint intersections were not permitted in practice.

The four joint configurations considered in the study are the uniplanar K(N)-joints with and without gap, 100% overlapped and completely overlapped joint (Fig. 21). The dimensional, geometrical, and material properties as well as the boundary conditions of the four joint configurations are identical, as summarised in Fig. 22. In the analysis, eight load cycles were applied to simulate the cyclic loading, and the joint deformation was set at two times the excessive deformation limit specified by Yura et al. (1980).

The axial load-displacement hysteresis curves of the four joint configurations are plotted in Fig. 23. It was not unexpected that the 100% overlapped tubular joint presented the highest strength and initial stiffness. The completely overlapped joint yielded larger but smaller compressive strength compared to the joint with and without gap. A similar
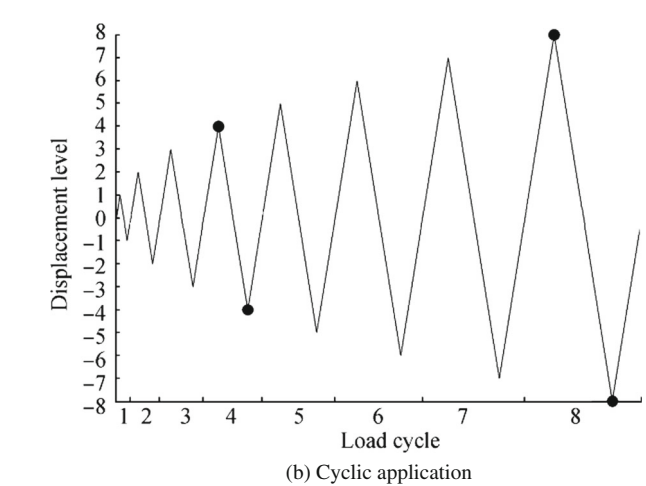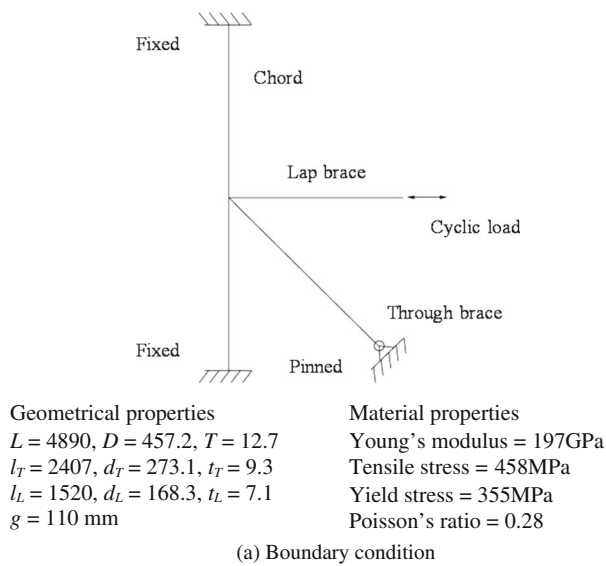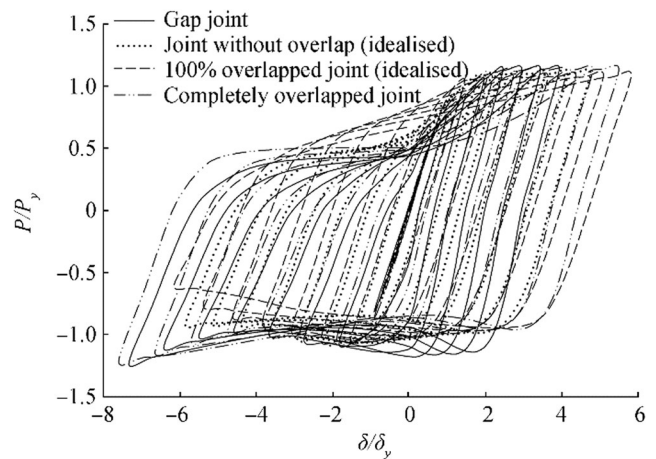

Fig. 23 Comparison of hysteresis curves

behaviour of the joints in tension phase of the hysteresis curves was noted. In the compression phase, the completely overlapped joint showed a more stable hysteresis behaviour than the gap joint. Bur in the tension phase, the 100% overlapped joint performed better. However, its strength in the compression phase deteriorated more severe than other joint configurations due to the lap brace member failure.

The completely overlapped joint dissipates more energy than the 100% overlapped joint and the joint with and without gap, with a difference of 6%, 18%, and 32%, respectively (Fig. 24). The joint also demonstrated a better ductility performance with an accumulative ductility ratio of 9.3%, 16.2%, and 23.4% more than that of the 100% overlapped joint and the joint with and without gap, respectively (Fig. 25).

For strength resistance, the compressive and tensile capacity of completely overlapped joint is closed to that of the joints with and without gap (Fig. 26). All the joint configurations demonstrated similar tensile strength resistance at large load cycles. The strength of 100% overlapped joint in compression deteriorated due to lap brace buckling. On the contrary, the completely overlapped joint and the gap joint showed increase of compressive resistance due to bending stiffness of chord

Geometrical properties
$L = 4890, D = 457.2, T = 12.7$
$l_T = 2407, d_T = 273.1, t_T = 9.3$
$l_L = 1520, d_L = 168.3, t_L = 7.1$
$g = 110$ mm

Material properties
Young's modulus = 197GPa
Tensile stress = 458MPa
Yield stress = 355MPa
Poisson's ratio = 0.28

(a) Boundary condition

(b) Cyclic application

Fig. 22 Properties of four (4) joint configurations. **a** Boundary condition. **b** Cyclic application
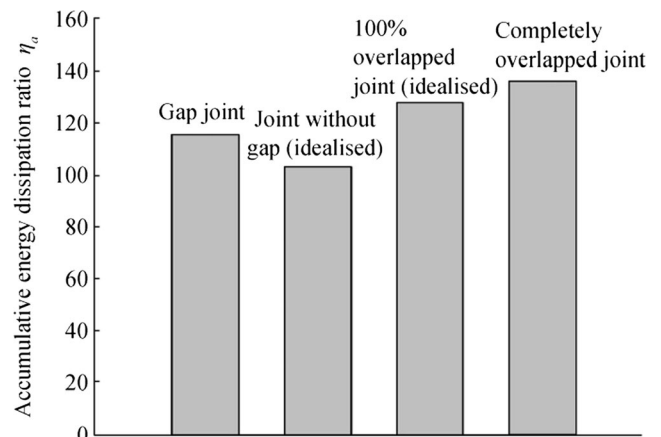

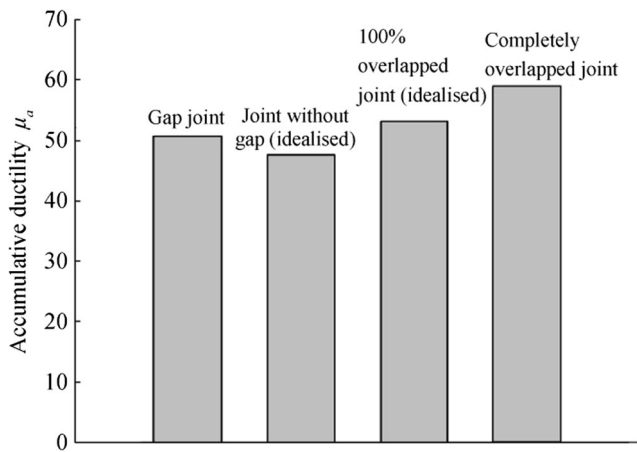Fig. 24 Comparison of energy dissipation capacity

Fig. 25 Comparison of ductility ratio

member at large displacement, in the later phase of load cycles.

From the stress distribution depicted in Fig. 27, the maximum von Mises stress of the gap joint is concentrated on the chord face, on the gap region between the two braces. This was not unexpected as the load was transferred between the two braces via the punching shear and shell bending action of the gap element. For the joint without gap, the load was mainly transmitted by the shear effect of the chord wall between the braces. For the 100% overlapped joint, the load was 100% transferred between the braces without passing through any gap element at the joint. This joint appeared to be rigid with a high diameter ratio between the two braces. Owing to limited localised deformation, the overlapped brace might contact the chord wall in the process of load transfer between the two braces. Similar to the behaviour of 100% overlapped joint, the load of the completely overlapped joint was 100% transferred directly between the two braces. However, the main difference from the 100% overlapped joint was that the damage of the completely overlapped
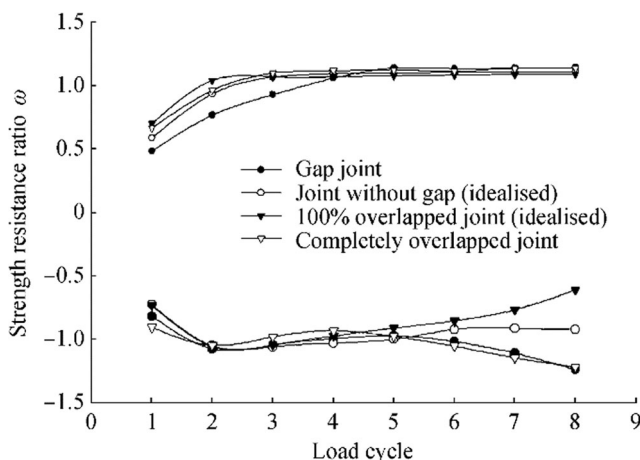

(a) Gap joint (b) Joint without gap
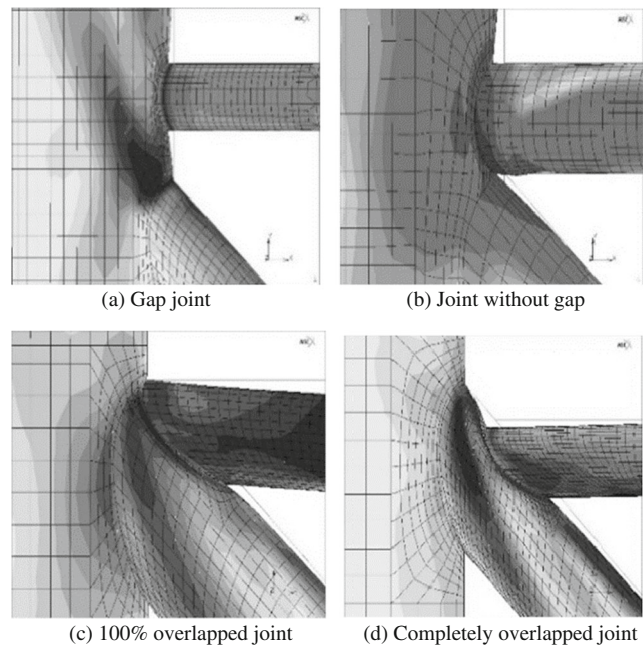(c) 100% overlapped joint (d) Completely overlapped joint

Fig. 27 Equivalent stress distribution of K(N)-joints

joint is located at the short segment of the diagonal through brace and not at the chord wall.

In summary, it could be commented based on the observation from the load transfer mechanism that the completely overlapped joint performed better to contain the damage, with an inelastic yielding and local buckling of the short segment member, than the conventional gap joint with chord wall failure. This implied that in the event of intense earthquake or environmental forces, the chord member of the completely overlapped joint could remain intact without severely damage or collapse.

7 Conclusions

The evaluation of cyclic behaviour of completely overlapped joint is performed based on the experimental and numerical study. The test of the joint specimens is carried out to verify the reliability of the FE model for detailed analysis. The accuracy of the joint model is further justified with respect to the effect of its finite element type, weld element, material property, and failure criterion. The results showed that the four-node thick shell element was suitable for modelling the joint. The impact of modelling the weld element at joint connections was minimal. For the material property, the material kinematic hardening rule simulated very well the post yield behaviour of the joint.

Apart from the advantages of being easy-to-fabricate with reduced fabrication cost due to reduced number of welded joints and shorter thicker wall cans at joint connections, it also demonstrated from the cyclic behaviour that the completely

Fig. 26 Comparison of strength resistance

overlapped joint performed better with higher strength resistance, stiffness, ductility, and energy absorption capacity than the conventional gap joint commonly found in typical X-braced jacket substructures.

Unlike the conventional gap joint with the maximum stress on the chord wall, the maximum stress of the completely overlapped joint is located at the short segment of the diagonal through brace. The inelastic yielding and local buckling failure behaviour of the short segment member suggested that the eccentric jacket with completely overlapped joint could be designed effectively in accordance with the strength and ductility requirements so as to prevent the collapse of wind turbine in the event of intense earthquake and environmental forces.

References

American Petroleum Institute, API RP2A (2000) Recommended practice for planning, designing and constructing fixed offshore platforms, American Petroleum Institute, Washington, D. C, USA

American Welding Society, AWS (2000) Structural welding code–steel, ANSI/AWS, D1.1-2000, American Welding Society, Miami, USA

British Standard Institution, BSI (1998) Metallic materials-tensile testing, BS EN 10002-1:1990, British Standard Institution, London

Canadian Standards Associations, CSA (1989) Steel structures for buildings, limit states design, CAN-CSA S16.1, Canada

Cheung LY, Gho WM, Fung TC, Soh CK (1998) Design economics of offshore structure - eccentric jacket. Journal Institution of Engineers, Singapore 138(3):42–49

European Convention for Constructed Steelwork, ECCS (1986) Recommended testing procedure for assessing the behaviour of structural steel elements under cyclic loads, European Convention for Constructed Steelwork Technical Committee 1—Structural Safety and Loadings, Technical Working Group 1.3- Seismic Design

Fung TC, Soh CK, Gho WM, Qin F (2001) Ultimate capacity of completely overlapped tubular joints I: an experimental investigation. J Constr Steel Res 57(8):855–880. https://doi.org/10.1016/S0143-974X(01)00013-X

Gao F, Gho WM (2008) Parametric equations to predict SCF of axially loaded completely overlapped tubular circular hollow section joints. J Struct Eng ASCE 2008(3):412–420 https://ascelibrary.org/doi/abs/10.1061/(ASCE)0733-9445(2008)134:3(412)

Gao F, Hu B, Zhu HP (2013) Parametric equations to predict LJF of completely overlapped tubular joints under lap brace axial loading. J Constr Steel Res 89:284–292. https://doi.org/10.1016/j.jcsr.2013.07.010

Gho WM (2009) Local joint flexibility of tubular circular hollow section joints with complete overlap of braces. Proceedings of Tubular Structures XII, Shanghai, China, 607–614

Gho WM, Yang Y (2005) Cyclic performance of completely overlapped tubular joints. Proceedings of The 15th International Offshore and Polar Engineering Conference, ISOPE, Seoul, Korea, 320–324

Gho WM, Yang Y (2008) Parametric equations for static strength of tubular circular hollow section joints with complete overlap of braces. J Struct Eng ASCE 2008(3):393–401 https://ascelibrary.org/doi/abs/10.1061/(ASCE)0733-9445(2008)134:3(393)

Gho WM, Fung TC, Soh CK (2003) Stress and strain concentration factors of completely overlapped tubular K (N)-joints. J Struct Eng ASCE 129(1):21–29 https://ascelibrary.org/doi/abs/10.1061/(ASCE)0733-9445(2003)129:1(21)

Gho WM, Yang Y, Gao F (2006) Failure mechanism of tubular CHS joints with complete overlap braces. Thin-Walled Struct 44(2006):655–666. https://doi.org/10.1016/j.tws.2006.05.007

MARC (2000) User information. Volume A, MARC Analysis Research Corporation, California, USA

New Zealand Standard, NZS (1992) Code of practice for general structural design and design loading for buildings, and commentary, Part1, 2, NZS 4203, Standards Association of New Zealand, Wellington, New Zealand

Soh CK, Fung TC, Qin F, Gho WM (2001) Behaviour of completely overlapped tubular joints under cyclic loading. J Struct Eng ASCE 2001(2):122–128 https://ascelibrary.org/doi/abs/10.1061/(ASCE)0733-9445(2001)127:2(122)

Yang Y (2006) Behaviour study of completely overlapped tubular joints under monotonic and cyclic axial loading. Ph.D. thesis, Nanyang Technological University, Singapore

Yeter B, Garbatov Y, Guedes Soares C (2016) Evaluation of fatigue damage model predictions for fixed offshore wind turbine support structures. Int J Fatigue 87:71–80. https://doi.org/10.1016/j.ijfatigue.2016.01.007

Yura JA, Zettlemoyer N, Edwards IF (1980) Ultimate capacity equations for tubular joints. Offshore Technology Conference, OTC 3690, Houston: 113–127. https://doi.org/10.4043/3690-MS